

Ultrasound Imaging of Apoptosis in Tumor Response: Novel Preclinical Monitoring of Photodynamic Therapy Effects

Behzad Banihashemi,^{1,3} Roxana Vlad,^{2,4} Branislav Debeljevic,^{4,6} Anoja Giles,⁴ Michael C. Kolios,^{2,5,6} and Gregory J. Czarnota^{1,2,3,4,5}

Departments of ¹Radiation Oncology and ²Medical Biophysics, Faculty of Medicine, University of Toronto; Departments of ³Radiation Oncology and ⁴Imaging Research, Sunnybrook Health Sciences Center; Department of ⁵Physics and ⁶Electrical and Computer Engineering, Ryerson University, Toronto, Ontario, Canada

Abstract

High-frequency ultrasound is a novel method to detect apoptotic cell death based on changes in cell morphology that cause alterations in the viscoelastic and, consequently, the acoustic properties of cell ensembles and tissues. In this study, we evaluated the first preclinical tumor-based use of high-frequency ultrasound spectroscopy to noninvasively monitor tumor treatment by following xenograft malignant melanoma tumor responses to photodynamic therapy (PDT) *in vivo*. We observed a time-dependant increase in ultrasound backscatter variables after treatment. The observed increases in spectroscopic variables correlated with morphologic findings, indicating increases in apoptotic cell death, which peaked at 24 hours after PDT. We analyzed the changes in spectral slope and backscatter in relation to apoptosis and histologic variations in cell nuclear size. Changes in spectral slope strongly correlated with the changes in mean nuclear size over time, associated with apoptosis, after PDT ($P < 0.05$). At 48 hours, a decrease in ultrasound backscatter was observed, which could be explained by an increase in cell nuclear degradation. In summary, we show that high-frequency ultrasound spectroscopic variables can be used noninvasively to monitor response after treatment in a preclinical tumor cancer model. These findings provide a foundation for future investigations regarding the use of ultrasound to monitor and aid the customization of treatments noninvasively based on responses to specific interventions. [Cancer Res 2008;68(20):8590–6]

Introduction

Ultrasound has been used successfully in medical imaging for many years because it is safe, real-time, noninvasive, and relatively inexpensive. A transducer emits a high frequency acoustic wave that propagates through tissue. Part of this wave is scattered back by the acoustic inhomogeneities inside the tissue and can be displayed as an ultrasound image or gathered as a spectrum of radiofrequency data. Ultrasonic scattering in biological tissues is a complex process. It is primarily affected by the acoustic impedance and the size of tissue scattering structures in relation to the ultrasound wavelength. Ultrasonic tissue signal changes are based on the foundation that pathologic or therapeutic processes alter

physical characteristics of tissue, such as compressibility, density, and geometry of scatterers, and these alterations cause observable changes in acoustic scattering properties (1). High-frequency ultrasound has been classically used to monitor tumor size changes in preclinical metastatic models of cancer (2, 3). Such physical characteristics of ultrasound make it a very attractive tool to monitor changes in tumors in response to treatment. Based on these principles, high-frequency ultrasound has been used to monitor structural changes at the cellular level *in vitro* (4) and *in vivo* (1, 5), because it permits imaging at resolutions higher than that offered by conventional ultrasound. In this study, we show, for the first time, that preclinical spectroscopic ultrasound analyses can noninvasively detect time-dependent, photodynamic therapy (PDT)-induced apoptotic cell death in tumors *in vivo*.

Apoptosis or programmed cell death plays a significant role in normal and pathologic processes in biology (6), as well as in response to therapeutic interventions (7) in oncology. During apoptosis, cells die in an organized and energy-dependent fashion. Striking structural changes occur; the nucleus coalesces, seems condensed, and subsequently fragments, and the cellular membrane undergoes extensive changes, called blebbing (8). Currently, standard biological methods for detecting apoptosis are invasive and time consuming, involving a sample biopsy and special staining. A number of imaging-based methods that can detect tumor responses to treatment have been recently developed, as reviewed in Brindle (9). These include 2-[¹⁸F]fluoro-2-deoxy-D-glucose positron emission tomography (PET) and [¹³C]hyperpolarized pyruvate imaging as makers of tumor glucose metabolism, 3'-deoxy-3'-¹⁸F flurothymidine for DNA synthesis, and PET and magnetic resonance spectroscopy for amino acid and lipid metabolism (reviewed in ref. 9). Furthermore, tumor cell death, now recognized to be a good prognostic indicator of outcome (reviewed in ref. 9), can be detected using magnetic resonance techniques and antibody-based labeling imaging using single-photon emission computed tomography, PET, and MRI and optical imaging (reviewed in ref. 9). Czarnota and colleagues have shown that high-frequency ultrasound techniques are exquisitely sensitive to detect the morphologic changes associated with the apoptotic process (4, 5, 10, 11). In those experiments, it was shown, using packed acute myeloid leukemia (AML) cells treated with an apoptosis-inducing drug, that an increase of 9 to 13 dB in backscatter amplitude could be detected with high-frequency ultrasound. Their most recent studies have indicated that this method can be used to detect as little as 5% apoptosis in a well-controlled cell culture model. This places ultrasonic detection of cell death in a potentially clinically relevant domain where tumor masses typically show an apoptotic index between 2% and 20% with up to 2-fold increases with cancer treatments. High-frequency ultrasound spectral variables have been successfully used to

Note: Supplementary data for this article are available at Cancer Research Online (<http://cancerres.aacrjournals.org/>).

Requests for reprints: Gregory J. Czarnota, Department of Radiation Oncology, University of Toronto and Sunnybrook Health Sciences Center, 2075 Bayview Avenue, Toronto, Ontario, Canada M4N 3M5. Phone: 416-480-5329; Fax: 416-480-6002; E-mail: Gregory.Czarnota@sunnybrook.ca.

©2008 American Association for Cancer Research.
doi:10.1158/0008-5472.CAN-08-0006

monitor apoptosis *in vitro* with AML cell pellets (10) and *in vivo* in liver tissue during preservation (1). It is believed that the sensitivity to apoptosis in high-frequency ultrasound images and spectra is linked to changes in nuclear structure, as changes in nuclear size and nuclear condensation significantly change ultrasound backscatter (5, 12, 13).

PDT is a minimally invasive, evolving therapeutic modality in cancer treatment. A photosensitizer catalyzes, upon irradiation, formation of reactive oxygen species that causes the cytotoxic effect in tissue. In 1991, Oleinick and colleagues showed that PDT could trigger a rapid induction of apoptosis in a lymphoma cell line (14). Subsequently, apoptosis has been shown to be a rapid and dominant form of cell death after PDT in a multiple experimental setting using a variety of cell types by an array of different sensitizers (15–17). Czarnota and colleagues showed the ultrasonic detection of apoptosis *ex vivo* in rat brain and *in vivo* in skin after PDT (5). In that study, they presented the results of the first study aimed at detecting apoptosis in non-tumor-bearing tissues after PDT. In this study, we are presenting preclinical proof-of-principle research that high-frequency ultrasound can be used *in vivo* to monitor tumor cell death responses, in this case, using photodynamic therapy in xenograft malignant melanoma tumors non-invasively as a model of tumor death.

Materials and Methods

Solid tumors were grown in SCID mice using a malignant human melanoma cell line HTB-67 (American Type Culture Collection). Tumor cells, in volume of 50 μ L, were injected intradermally at a concentration of $10^4/\mu$ L. After the tumor grew to 7 to 10 mm in diameter, mice were given 10 mg/kg of Photofrin (QLT) as a photosensitizer, injected *i.p.* Animals were then kept in a dark environment for 24 h before irradiation with light. Tumors were then treated with 110 J/cm² of 633 nm laser light, with a focal spot of 3-mm diameter targeted on half the tumor for 30 s. Each tumor thus served as its own control. Tumors were examined by 26 and 40 MHz high-frequency ultrasound before irradiation and at selected times and then processed for histologic examination. Animals were examined at 1, 3, 6, 12,

24, and 48 h after PDT with three animals used for each time point for ultrasound and histologic examination. Two additional animals served as sham controls with the total of 20 animals in these experiments.

For histologic analysis, tumors were sectioned and stained with H&E. To specifically assess apoptotic cell death, the TdT-mediated dUTP-biotin nick end-labeling (TUNEL) assay was performed. Light microscopy was carried out, and digital images were analyzed using Image J software (NIH). ImageJ was used to estimate total tumor area, the gross apoptotic area from TUNEL stained images, and to measure average nuclear size in the treated area. For each tumor sample, the data were collected from three different regions of the treated area and averaged for the final analysis (nine regions of interest for each experimental time).

Ultrasound data collection consisted of acquiring B-scan images in addition to spectroscopic RAW radiofrequency data for quantitative analyses of backscattered ultrasound. Forty-eight hours after depilatory hair removal, living animals were imaged using high-viscosity ultrasound gel (ATL, Inc.) as coupling agent over the skin in tumor-bearing areas. We used a radiofrequency-enabled ultrasound machine (VisualSonics VS40B) coupled with an F2 transducer operating at 26 MHz. This transducer produces a practical frequency range of 20 to 32 MHz (\pm 6 MHz band width) and has much better signal to noise characteristics compared with 40 MHz data, which was also collected, but not consequently used extensively. The focal depth of the instrument was set at 3 mm, and for the 26-MHz transducer, its axial resolution was 58 μ m and its lateral resolution, limited by the ultrasound beam width, was 60 μ m. For data collection, the ultrasound transducer was positioned such that the focal zone was at the same depth in each imaged specimen to control for any potential attenuation. All images and radiofrequency data were digitally recorded. We chose a region of interest (ROI) in ultrasound images that represented the treated half of the tumor (approximate size of 3 \times 3 mm) and was centered approximately at the focal depth of the transducer. Three representative ROIs were selected for each tumor sample and averaged for the final analysis. The spectroscopic data were studied by using backscattered radiofrequency data from individual scan lines using customized MATLAB computer software written in-house (The Math-Works). The backscatter spectrum was normalized by the spectrum of the echo from a Quart flat calibration target (EFSTON Sciences; refs. 11, 18). This was carried out to remove system and transducer transfer functions to provide a common reference frame for collected data. Linear regression

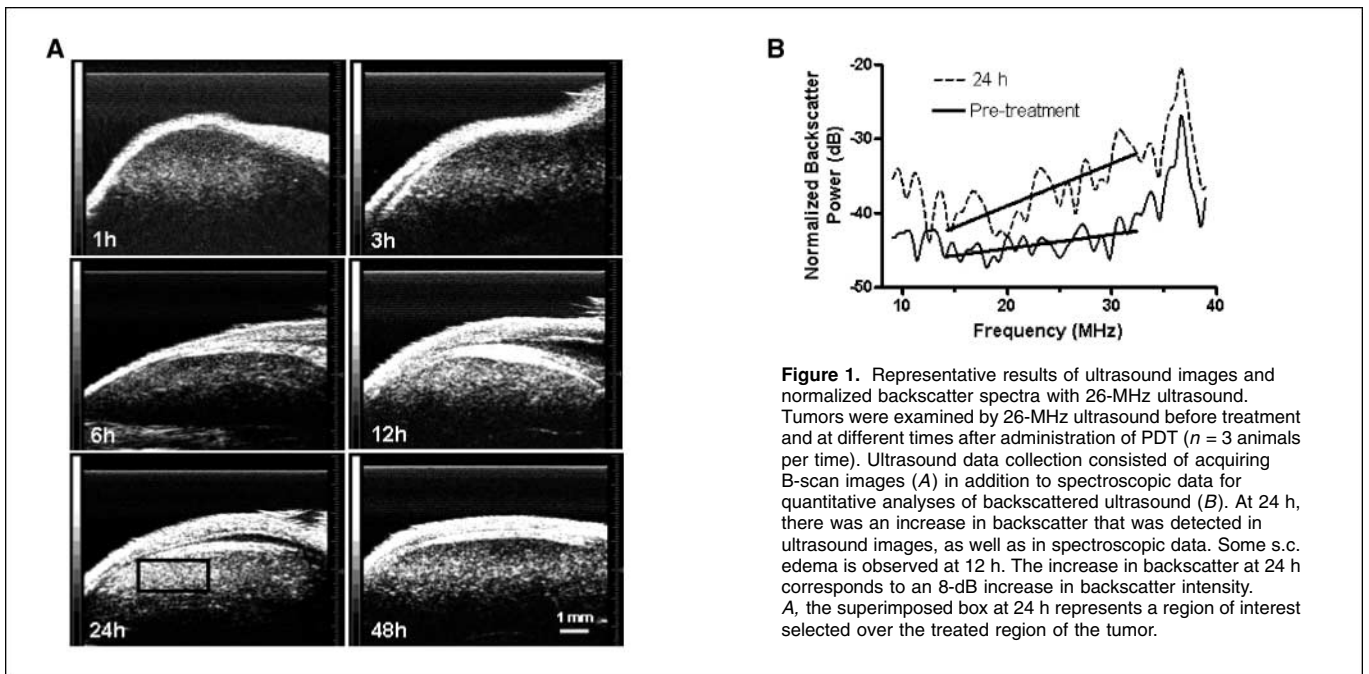


Figure 1. Representative results of ultrasound images and normalized backscatter spectra with 26-MHz ultrasound. Tumors were examined by 26-MHz ultrasound before treatment and at different times after administration of PDT ($n = 3$ animals per time). Ultrasound data collection consisted of acquiring B-scan images (A) in addition to spectroscopic data for quantitative analyses of backscattered ultrasound (B). At 24 h, there was an increase in backscatter that was detected in ultrasound images, as well as in spectroscopic data. Some s.c. edema is observed at 12 h. The increase in backscatter at 24 h corresponds to an 8-dB increase in backscatter intensity. A, the superimposed box at 24 h represents a region of interest selected over the treated region of the tumor.

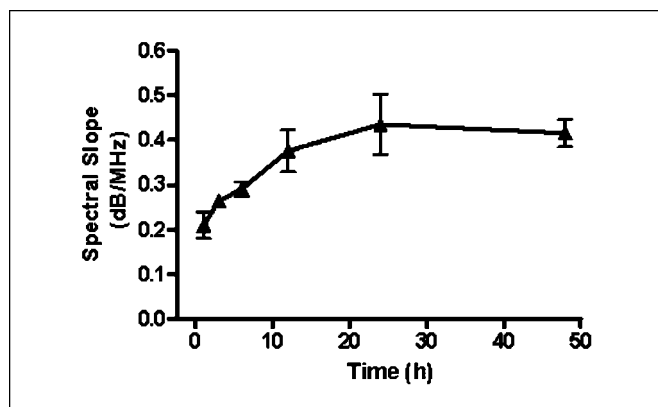


Figure 2. Plot of calculated spectral slope as the function of time after photodynamic therapy with 26-MHz ultrasound. Radiofrequency data collected in the time course experiments were analyzed and plotted. Points, average of spectral slopes for three animals for each experimental time; bars, SD. Three regions of interest were measured and analyzed in each animal (total of nine measurements for each experimental time).

analysis was applied to the normalized spectral data to provide a best-fit line (11, 18). The backscatter spectrum was obtained by averaging the result from nominally 20 independent scan lines within representative regions of interest.

To assess the role of ultrasound spectroscopic analysis to monitor photodynamic therapy, we measured two variables from 26-MHz transducer data in the backscattered spectra: spectral slope and midband fit (MBF). Spectral slope is the slope of the linear regression of the calibrated spectrogram, and MBF is the value of the regression fit at the center frequency over which the spectrum was analyzed. These variables can potentially be mathematically related to physical characteristics of ultrasound scatterers, such as scatterer size and scatterer concentration (11, 18–20). We then carried out a correlation of these data with histologic variables of measured cell death in these experiments. Because the 26-MHz transducer has a broad bandwidth and is still sensitive to 10 MHz, we also evaluated limited (MBF) changes in the lower frequency range, as our previous *in vitro* work also evaluated this region (11).

We also probed the significance of nuclear changes by performing experiments *in vitro* using an AML system as before (5). Nuclei from viable and 20-h cisplatin-treated apoptotic cells were isolated (12), and each was suspended in room-temperature PBS at 5.6×10^6 nuclei/mL. Ultrasound data were collected as before (12) using a wide-band 20-MHz transducer and analyzed as above.

Results

Ultrasound analysis. Before and at specified times after treatment, images and backscattered ultrasound data were collected for each mouse. Photodynamic treatment produced constant and reproducible changes in ultrasound images and spectral variables as a function of time after exposure (Fig. 1). Figure 1A shows a series of representative conventional B-scans after PDT at specified times. We observed a consistent increase in backscatter intensity as a function of time that reached its maximum within 12 to 24 hours of treatment and decreased subsequently at 48 hours. Figure 1B shows a representative sample of normalized spectroscopic ultrasound changes that were observed in which normalized power spectrum is plotted over the -6 dB bandwidth of the transducer. The best-fit line to the spectra was used to extract the spectroscopic variables for each ROI, which was selected in the treated regions of the tumor knowing where PDT was applied. As shown in Fig. 1B, at 24 hours after treatment, an increase in the spectral slope and MBF was

observed. In the sections that follow, we discuss the results for each of the variables separately.

In our experiments using the 26-MHz frequency ultrasound and a -6 dB effective band width of 19 to 32 MHz, the spectral slope in the backscattered spectra was measured as 0.156 ± 0.02 dB/MHz in the tumors before treatment. The spectral slope increased as a function of time after photodynamic therapy and reached its maximum at 24 hours (0.435 ± 0.07 dB/MHz; Fig. 2). In those experiments, the average value of spectral slopes in dB/MHz were measured as increasing from 0.21 ± 0.03 to 0.41 ± 0.01 from 1 to 48 hours, respectively. The spectral slope is an indicator of effective scatterer size and an increase in slope has been shown to correspond to a decrease in effective scatterer size (11). The observed changes in the spectral slope over time after photodynamic therapy could be suggestive of the structural changes in the tumor cells after treatment, namely apoptotic nuclear coalescence, condensation, and fragmentation.

Using 26-MHz ultrasound, we observed a significant increase in the MBF variable after exposure to photodynamic therapy. At 12 hours, the average MBF increased from -41.1 ± 2.5 to -31.9 ± 1.4 dBr. This 9.2 ± 1.1 dB increase in MBF translated to almost eight times enhancement in the MBF intensity compared with pretreatment variables. Figure 3 shows changes in MBF as a function of time after treatment. We detected a consistent increase in MBF over time in all treated animals after PDT with maximum values occurring at 12 to 24 hours. The MBF is representative of the ultrasound backscatter and depends on the scatterer shape, size, acoustic impedance, spatial distribution, and concentration (11). The observed increase in the MBF after photodynamic treatment can provide an insight into the structural and organizational alterations that happen in tissue after treatment. Data at 40 MHz were typically consistent in trend but noisier due to the superior signal-to-noise ratio obtained at 26 MHz. Examination of the 10 to 15 MHz bandwidth of the data from the 26-MHz transducer indicated a similar trend of increase in MBF with treatment time. At 1, 3, 6, 12, 14, and 48 hours compared with before treatment increases of 0.9 ± 0.3 , 0.4 ± 0.3 , 2.8 ± 0.5 , 5.1 ± 1.5 , 3.2 ± 1.1 , and 1.5 ± 1.3 dB in MBF were observed with values approximately half of that at the higher frequencies (Fig. 3).

Histologic analysis. Figure 4 illustrates the representative histologic results at specified time points after photodynamic

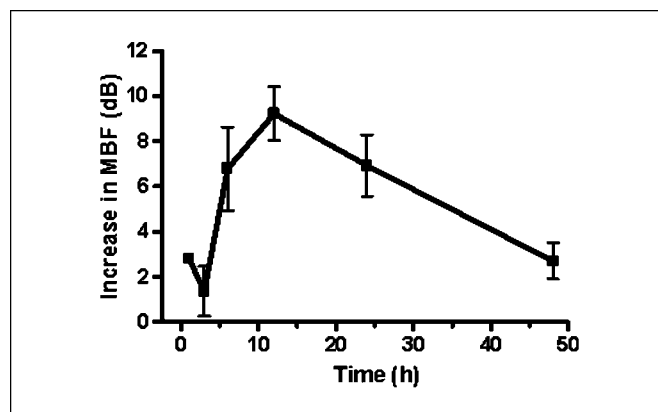


Figure 3. Increase in MBF as a function of time after PDT detected by 26-MHz ultrasound. Points, average of MBF for three animals at each experimental time; bars, SD. Three regions of interest was measured and analyzed in each animal (total of nine measurements for each experimental time). A maximum increase of 9.2 dBr was observed at 12 h. This translates to about eight times increase in backscatter intensity compared with untreated tumors.

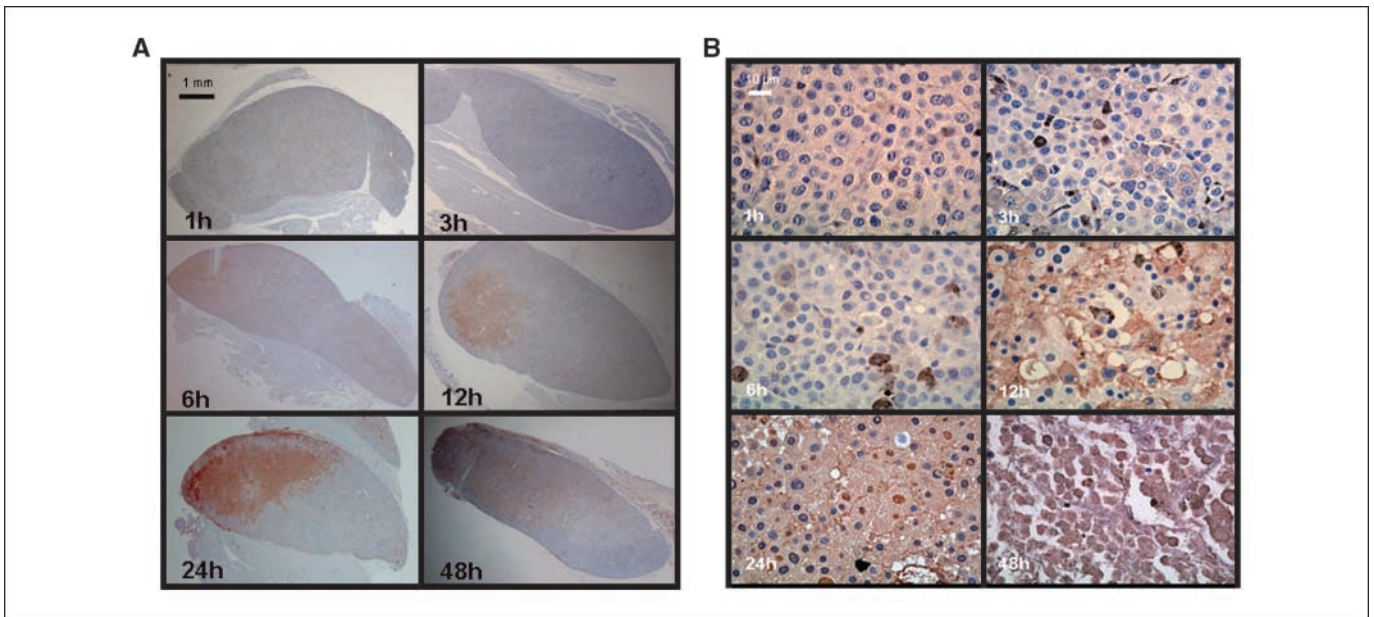


Figure 4. Representative results of histology data prepared by TUNEL staining with low (2.5×; A) and high (40×; B) magnification at specific time points after photodynamic therapy. Area of apoptotic cell death (brown) was measured as a percentage of the tumor surface area using Image J software. In the treated area, apoptosis achieved to its highest level at 24 h, and then cellular lysis and nuclear disintegration were observed. With higher magnification, we observed typical changes of apoptosis, including nuclear coalescence and fragmentation, as the function of time. At 48 h, nearly half of the cells in the treated area have lost their nuclei as in a final stage of apoptotic cell death. These changes explain the detected changes in variables related to the size of scatterers in the tissue by ultrasound.

therapy. TUNEL staining (current histologic gold standard for detecting apoptotic cell death) showed dominant cell death in treated areas that increased considerably over time and reached a maximum at 24 hours (Fig. 4A). The average gross apoptotic region involved 3%, 27%, 52%, and 34% of the tumor area at 6, 12, 24, and 48 hours after treatment, respectively. Meanwhile, at higher magnification (Fig. 4B), extensive changes in morphology were observable in the treated area, including blebbing changes in cellular membrane, nuclear coalescence, and nuclear fragmentation. The percentage of TUNEL-positive cells in the treated area increased from <3% at 0 and 1 hours to an average of 12%, 51%, 45%, and 32% at 6, 12, 24, and 48 hours after photodynamic therapy (Table 1). At 48 hours, a significant portion of cells were observed to have entered the final phases of cell death as documented by extensive nuclear digestion and cell degradation (Fig. 4B). At 48 hours after treatment, on average, nearly 50% of the cells in the treated area appeared with their nuclei not visible (Table 1). These alterations were a strong indication of a dominant apoptotic cell

death that occurred very rapidly after photodynamic therapy within a few hours in our experimental conditions and peaked at 12 to 24 hours. Other investigators have also found a similar response to PDT in regard to timing and extent of apoptosis (16).

Nuclear coalescence and fragmentation were observed as hallmarks of apoptotic cell death. Coincidentally, there is a strong argument in the literature that suggests the cell nucleus as a strong source of ultrasonic scattering in cell assemble and tissue (4, 5, 10). We, thus, measured the average nuclear size in the treated area in our tumors before treatment and after PDT (Table 1). Forty-eight hours after treatment, mean nuclear size decreased to almost one third of the original size, from 56 μm^2 in cross-sectional area before treatment to 35, 23, and 20 μm^2 cross-sectional area at 12, 24, and 48 hours, respectively. This gradual and considerable decrease in mean nuclear size was consistent with the expected nuclear changes during apoptosis. The changes in mean nuclear size strongly correlated statistically with the alterations in ultrasonic spectral slope with a Spearman *R* factor of -0.89 ($P = 0.03$).

Table 1. Histologic findings in treated areas of tumors after treatment with photodynamic therapy at different time points

Time	0 h	1 h	3 h	6 h	12 h	24 h	48 h
% Apoptotic region	0	0	2 ± 1	3 ± 1	27 ± 2	52 ± 16	34 ± 12
% Apoptosis (TUNEL+)	2 ± 1	3 ± 1	9 ± 2	12 ± 1	51 ± 4	45 ± 7	32 ± 4
% Cell lysis/degradation	0	0	0	0	5 ± 3	10 ± 5	50 ± 10
Mean nuclear area (μm^2)	56 ± 5	54 ± 4	55 ± 1	44 ± 2	35 ± 1	23 ± 2	20 ± 2

NOTE: Percentage apoptotic region was determined as the TUNEL-positive area expressed as a percentage of tumor section area. This value reached to its highest level at 24 h after photodynamic therapy. Percentage apoptosis was measured by counting TUNEL-positive cells in respect to total cells in each microscope field (20×) magnification. Percentage of cells lysed was assessed by counting cell lysis or complete nuclear digestion in each field (magnification, 20×). We evaluated mean nuclear size by using Image J software. Each number represents an average from three animals at each experimental time. Three different areas were selected in each tumor (making a total of nine measurement areas for each experimental time).

In vitro results. Backscatter for nuclei from apoptotic cisplatin-treated AML cells exhibited a 6 to 8 dB increase compared with backscatter from viable AML cells for equivalent concentrations of nuclei over a 10 to 35 MHz frequency range (see supplementary data).

Discussion

This study has shown in a preclinical tumor model for the first time that high-frequency ultrasound spectroscopy can noninvasively monitor tumor response to treatment, in this case, photodynamic therapy. We have been able to show that different spectroscopic variables in ultrasound backscatter can be related to tumor physical characteristics in response to this therapeutic intervention by analyzing two main variables in the backscattered ultrasound (spectral slope and MBF). This work follows experiments conducted *in vitro*, *in situ*, and *in vivo* previously which did not use tumor models. In those experiments, Czarnota and colleagues observed more than a 2-fold increase in ultrasound backscatter in apoptotic cells compared with viable cells *in vitro* (4). It was experimentally shown at that time that chromatin condensation with mitosis caused increases in backscatter, and limited DNase digestions of nuclear material in cells reversed this. This suggested that the highly condensed clusters of nuclear material in apoptotic cells contributed to the greater scattering of ultrasound associated with apoptotic cells (4, 5, 11, 12). In recent work (12), findings suggested that integrated backscatter, but not attenuation or speed of sound, is correlated with nuclear size. Our data here is consistent with those findings. We observed significant nuclear coalescence and fragmentation after photodynamic treatment that correlated with results of spectroscopic analyses. The mean nuclear size decreased to near one half in cross-sectional area at 24 hours after photodynamic therapy, which was linked with increased ultrasound backscatter at this experimental time. At 48 hours, we detected considerable degradation of cell nuclei that can potentially explain the reduction in the backscatter in those samples. This too was consistent with previous observations *in vitro* in which extensive nuclear degradation lead to backscatter decreases (4).

Our working model of ultrasound backscatter with cell death is that backscatter from nuclear changes with cell death can contribute significantly to the effect visualized here (alternatives discussed further below). There are multiple sources of experimental evidence suggesting the role of nuclear structure in potentially influencing significantly ultrasound backscatter signals. This evidence includes:

1. In highly cellular xenograft tumors, backscatter signals and spectra are identical to backscatter signals and spectra of centrifuged cell models that mimic the histologic packing of xenografts. Such packed cell models have no extracellular matrix and collagen present yet exhibit nearly identical ultrasound scattering profiles (21, 22).
2. Different cell types may be differentiated in part on the basis of their nuclear signals (12). This further suggests to us an important role of nuclear structure in backscattered ultrasound.
3. In cell experiments where nuclear structure is specifically modified, there are changes in backscattered ultrasound. We have previously shown that such changes specifically cause the types of backscatter changes we have been observing. When cells are treated with colchicine to arrest them in G₂-M of mitosis with condensed nuclear material, there are significant

- increases in backscattered ultrasound. We have shown that such increases are reversed by digesting cellular DNA through enzymatically treating such colchicine-treated cells with DNase (4). Additionally, if one similarly subjects viable cells or mouse liver tissue to enzymatic digestions with DNase, backscatter signals drop to at least half their pretreatment values (23).
4. Similarly, other experiments in which cells are treated with sodium butyrate to cause chromatin unfolding exhibit significant decreases in ultrasound backscatter (23).
 5. Calculated scatterer sizes from ultrasound backscatter do not work out to be the same as cell sizes but coincide with smaller sizes suggestive again of an important role of the nucleus (21, 22).
 6. Isolated nuclei from apoptotic cells compared with viable cells exhibit greater backscatter (supplementary data).

Alternative mechanisms for the changes detected here could potentially include partial loss of water by tissues or extracellular matrix cross-linking with treatment. Whereas, there may be a cellular redistribution of water as measured by MRI (24) and would likely not account on its own in the absence of nuclear morphologic changes for the consistent spectral and ultrasound backscatter changes associated with cell death. In addition, the ultrasound changes detected here are not treatment modality or melanoma tumor-specific and are similar to those detected with chemotherapy in preclinical mouse tumor lymphoma models and radiation therapy in a number of preclinical xenograft tumor models (25, 26).

MRI has been used to study apoptosis on the basis that cells dying by this process undergo modifications in water content. Most studies published rely on gadolinium to probe water content changes (27, 28). *In vivo* any primary signal changes associated with apoptotic cells in tissue parenchyma would be potentially convoluted with signal changes caused by differences in vascular permeability to gadolinium that may occur with vascular cell death. Specific approaches have relied on gadolinium chelates of the C2A domain of synaptotagmin-I that binds to phosphatidyl serine exposed on apoptotic and apo-necrotic cell membranes (29). Other new approaches rely on measurements of intracellular sodium with MRI and have found this to correlate to taxotere chemosensitivity-induced regions of apoptosis (30). Other studies have shown the further utility of T1rho and T2rho MR imaging for apoptosis detection (31).

Morphology changes in cells undergoing apoptosis are also expected to result in changes in cellular elasticity and viscosity which potentially result in acoustic property changes. Micro-rheological methods (32–36) are one manner in which such changes can be assessed. Estimates that we have made using PC3 prostate cells exposed to 1 µg/mL cisplatin, which induces apoptotic cell death, indicate, after 9 to 12 hours of exposure, concomitant with nuclear condensation and the onset of fragmentation that the elastic modulus increased from 9 ± 2 Pa to 30 ± 5 Pa at a sampling of 3 radians/s, whereas the viscous modulus exhibited less of change.⁷

Photodynamic therapy can cause cross-linking of proteins, which could cause increases in tissue stiffness and could contribute to ultrasound backscatter changes (37–40). However, we expect such cross-linking changes to be temporally associated with the treatment and thus relatively rapid, whereas the changes we observe correlate with the slower progression of the development of apoptotic features of cells and their degradation after 48 hours. Any cross-linking that took place did not result in fixation and was

not sufficient to prevent cells from undergoing morphologic changes associated with cell death.

It has long been suggested that ultrasound backscatter variables may relate to physical tissue properties (17, 20). Ultrasonic spectral analysis techniques have been used by many investigators to add information to images generated by conventional ultrasound (10, 21, 22). Kolios and colleagues used ultrasound spectral analysis to measure changes in spectral slope and MBF in apoptotic cells *in vitro* (10). Significant increases in spectral slope and MBF in apoptotic cells were observed after exposure to chemotherapy that was in close agreement with theoretical predictions. This method was subsequently used in other experiments to assess apoptosis or other cellular structural changes *in vivo* (1, 11). Vlad and colleagues used ultrasound spectroscopic variables to noninvasively assess liver preservation injury in rats. In those experiments, they observed changes in spectroscopic backscatter in relation to liver ischemic injury induced by different storage conditions, including change in temperature or improper preservation (1). The study here investigated the use of spectral variables based on ultrasound backscatter data to monitor tumor response to photodynamic therapy. We observed a time-dependent change in MBF and spectral slope after treatment that correlated quantitatively with histologic changes in tumors. At 24 hours, the spectral slope doubled in value and MBF increased by almost 9 dB (approximately eight times increase in intensity), whereas the mean nuclear size decreased to half of its original value.

The spectral slope of the backscattered signal is related to the effective size of ultrasound scatterers (23). Our experiments support this theory *in vivo* in a tumor-bearing model after photodynamic therapy. Within the limits of our working hypothesis, an increase in spectral slope over time after treatment properly correlated with changes in mean nuclear size in the treated area. The process of nuclear coalescence and fragmentation is recognized to take place at early stages of apoptosis soon after treatment with photodynamic therapy (15). Our histologic data also support this rapid and dominant apoptotic process in this experimental setting. MBF is another measure of ultrasound backscatter. It depends on multiple factors, including scatterer size, concentration, and the acoustic impedance change between the acoustic scatterer and the surrounding medium (10). MBF increase could be due to the changes in nuclear scattering cross-section, a result of nuclear coalescence, or due to the alterations in randomization of the scatterer distribution due to nuclear fragmentation and condensation which can also affect backscatter. These theoretical and experimental avenues are under extensive evaluation.

In terms of theory, smaller nuclei, in the absence of nuclear condensation, provided all other physical properties remain the same, would reduce the scattering strength in our experiments. However, scattering strength depends not only on size but also differences in the mechanical properties of the scatterer and the surroundings (compressibility and density), number density of the scatterers (e.g., how many scatterers there are per unit volume), and, in the case of ultrasound for these wavelengths, the spatial distribution of the scatterers (whether more random or more ordered; refs. 12, 26). Our working model, that the nuclear condensation in combination with the cytoplasmic degradation increases the scattering strength of the individual nuclei during apoptosis, takes these factors into account supported by *in vitro*

experimentation. The *in vitro* experiments here (Supplementary Figs. S1–S3) in which backscatter differences for equivalent concentrations of nuclei from viable and apoptotic cells indicated a 6 to 8 dB greater backscatter power for apoptotic nuclei further support this interpretation. A more random organization of the scatterers *in vivo* could also increase the scattering strength given as ensemble of stronger scatterers. Also important is that with 25-MHz ultrasound and cells of size 10 to 30 μm , we are approaching the realm of Mie scattering, which complicates the analysis of the scattering strength with size due to ensemble effects. Given the pronounced nuclear degradation in the late stages of apoptosis, backscatter does diminish and has been observed not only in this study but in our original work (4). This is reflected in the 48-hour data in which an observed backscatter decrease correlates with almost complete nuclear degradation as evident in the corresponding histology, as expected.

Data were primarily obtained here at 25 MHz for analysis and presentation because of particular transducer characteristics which are optimal for preclinical imaging. We find that near 25-MHz one is able to obtain a better to signal-to-noise ratio due to the nature of transducer construction and there is far less attenuation of ultrasound than at higher frequencies. Consequently, the penetration in animal tumors was better with better overall images and signal statistics, although trends from data at 40 MHz (not shown) were similar. We have also analyzed data from the lower-band range of our 25-MHz transducer used here (10–15 MHz). These data indicated a lesser but detectable 6 dB increase in backscatter associated with cell death in this frequency range similar to that seen previously with a similar experimental system but *in vitro* samples (41). This frequency range approaches that of clinical ultrasound. Whether this phenomenon of cell death detection will be possible at clinical frequencies (1–10 MHz) still remains to be tested. From 10 to 15 MHz, the results are not surprising, mirroring previous *in vitro* experiments and falling into the realm of Rayleigh scattering as we are likely looking at the effect of stronger Rayleigh scatterers due to the nuclear condensation associated with cell death here.

In conclusion, high-frequency ultrasound can potentially serve well in the assessment of preclinical therapies. High-frequency ultrasound is comparatively an uncomplicated process for the visualization and assessment of xenograft tumors in mice or superficial regions, but clearly an alternative approach would be necessary with deeper tumors due to significant attenuation of high-frequency waves by tissue. Developments occurring in transducer technology should soon permit high-frequency transducers to be mounted on catheters or endoscopic probes which could aid in the imaging of deep lying structures and body cavities. Another alternative approach is to use the same principles of ultrasound spectroscopic analysis with conventional midfrequency ultrasound. Lower frequency ultrasound penetrates much deeper, and the backscattered data could be potentially subjected to the same analysis to provide information about structural changes in the tissue at the cellular level (41–46).

In summary, high-frequency spectroscopy was used to detect cell death in tumors treated by photodynamic therapy. These experiments were carried out as proof of principle to show the use of high-frequency ultrasound spectral methods to monitor structural changes in tumors in response to preclinical cancer treatment. Results showed a strong correlation between spectral variables and gold-standard histologic indicators of apoptotic cell death. Assessing tumor response and possibly predicting treatment outcome early in the course of cancer treatment may provide an opportunity

⁷ Kolios, unpublished data.

at the preclinical stage to accelerate the study of new therapeutic regimens and may be used potentially clinically in the future.

Disclosure of Potential Conflicts of Interest

M.C. Kolios and G.J. Czarnota: U.S. Patent on Detection of Apoptosis Using High-Frequency Ultrasound held by University Health Network. The other authors disclosed no potential conflicts of interest.

Acknowledgments

Received 1/2/2008; revised 7/22/2008; accepted 7/25/2008.

Grant support: This research was funded by the Canadian Institutes of Health Research (MOP grant 79447) and the National Sciences and Engineering Research

Council of Canada. The ultrasonic imaging device was purchased with funds from the Canada Foundation for Innovation, the Ontario Innovation Trust, and Ryerson University. Funding was also provided by Sunnybrook Health Sciences Centre, the University of Toronto Department of Radiation Oncology, and Canadian Association of Radiation Oncologist. This research was undertaken, in part, thanks to funding from the Canada Research Chairs Program awarded to M. Kolios and thanks to funding from the Ontario Ministry of Health and Long-term Care Clinician Scientist Programme awarded to G. Czarnota.

The costs of publication of this article were defrayed in part by the payment of page charges. This article must therefore be hereby marked *advertisement* in accordance with 18 U.S.C. Section 1734 solely to indicate this fact.

We would like to thank members of the Wilson laboratory at the Princess Margaret Hospital for assisting in the laser experiments. We thank Ralph Baddour and Lilian Doss for helpful contributions. We are grateful to Tennyson D. Bear for helpful discussions.

References

- Vlad RM, Czarnota GJ, Giles A, et al. High-frequency ultrasound for monitoring changes in liver tissue during preservation. *Phys Med Biol* 2005;50:197–213.
- Graham KC, Wirtzfeld LA, MacKenzie LT, et al. Three-dimensional high-frequency ultrasound imaging for longitudinal evaluation of liver metastases in preclinical models. *Cancer Res* 2005;65:5231–7.
- Wirtzfeld LA, Wu G, Bygrave M, et al. A new three-dimensional ultrasound microimaging technology for preclinical studies using a transgenic prostate cancer mouse model. *Cancer Res* 2005;65:6337–45.
- Czarnota GJ, Kolios MC, Vaziri H, et al. Ultrasonic biomicroscopy of viable, dead and apoptotic cells. *Ultrasound Med Biol* 1997;23:961–5.
- Czarnota GJ, Kolios MC, Abraham J, et al. Ultrasound imaging of apoptosis: high-resolution non-invasive monitoring of programmed cell death *in vitro*, *in situ* and *in vivo*. *Br J Cancer* 1999;81:520–7.
- Hockenbery D. Defining apoptosis. *Am J Pathol* 1995; 146:16–9.
- Debatin KM. Apoptosis pathways in cancer and cancer therapy. *Cancer Immunol Immunother* 2004;53:153–9.
- Allera C, Lazzarini G, Patrone E, et al. The condensation of chromatin in apoptotic thymocytes shows a specific structural change. *J Biol Chem* 1997;272:10817–22.
- Brindle K. New approaches for imaging tumour responses to treatment. *Nat Rev Cancer* 2008;8:94–107.
- Czarnota GJ, Kolios MC, Hunt JW, Sherar MD. Ultrasound imaging of apoptosis. DNA-damage effects visualized. *Methods Mol Biol* 2002;203:257–77.
- Kolios MC, Czarnota GJ, Lee M, Hunt JW, Sherar MD. Ultrasonic spectral parameter characterization of apoptosis. *Ultrasound Med Biol* 2002;28:589–97.
- Taggart LR, Baddour RE, Giles A, Czarnota GJ, Kolios MC. Ultrasonic characterization of whole cells and isolated nuclei. *Ultrasound Med Biol* 2007;33:389–401.
- Czarnota GJ. Ultrasound Imaging of Apoptosis *in vivo*: effects of subcellular nuclear structure and cell membrane morphology. Proceedings 10th Congress of the World Federation for Ultrasound in Medicine and Biology 2003;S117.
- Agarwal ML, Clay ME, Harvey EJ, Evans HH, Antunez AR, Oleinick NL. Photodynamic therapy induces rapid cell death by apoptosis in L5178Y mouse lymphoma cells. *Cancer Res* 1991;51:5993–6.
- Kessel D, Vicente MG, Reiners JJ, Jr. Initiation of apoptosis and autophagy by photodynamic therapy. *Autophagy* 2006;2:289–90.
- Nowis D, Makowski M, Stoklosa T, Legat M, Issat T, Golab J. Direct tumor damage mechanisms of photodynamic therapy. *Acta Biochim Pol* 2005;52:339–52.
- Oleinick NL, Morris RL, Belichenko I. The role of apoptosis in response to photodynamic therapy: what, where, why, and how. *Photochem Photobiol Sci* 2002;1:1–21.
- Lizzi FL, Greenebaum M, Feleppa EJ, Elbaum M, Coleman DJ. Theoretical framework for spectrum analysis in ultrasonic tissue characterization. *J Acoust Soc Am* 1983;73:1366–73.
- Feleppa EJ, Lizzi FL, Coleman DJ, Yaremko MM. Diagnostic spectrum analysis in ophthalmology: a physical perspective. *Ultrasound Med Biol* 1998;12: 623–31.
- Lizzi FL, Astor M, Feleppa EJ, Shao M, Kalisz A. Statistical framework for ultrasonic spectral parameter imaging. *Ultrasound Med Biol* 1997;23:1371–82.
- Vlad R, Ph.D. Thesis, University of Toronto; 2008.
- Oelze ML, O'Brien WD, Jr. Application of three scattering models to characterization of solid tumors in mice. *Ultrasound Imaging* 2006;28:83–96.
- Czarnota GJ, Kolios MC. Ultrasound imaging of apoptosis: role of chromatin structure and membrane configuration. Proc Am Inst Ultra Med Annu Meeting 2001;117.
- Bailey C, Giles A, Czarnota GJ, Stanisz GJ. Quantitative T1 and T2 relaxation in apoptotic cells in the presence of Gd-DTPA. *Proc Int Soc Mag Res Med* 2007;15:2833.
- Czarnota GJ, Chu W, Banihashemi B, et al. Quantitative ultrasound analyses of apoptotic cell death *in vivo* and histopathological correlations. Proc IEEE Ultrasonics Ferro-magnetics Frequency Control Annual Meeting Proceedings 2007.
- Hunt JW, Worthington AE, Xuan A, Kolios MC, Czarnota GJ, Sherar MD. A model based upon pseudo regular spacing of cells combined with the randomisation of the nuclei can explain the significant changes in high-frequency ultrasound signals during apoptosis. *Ultrasound Med Biol* 2002;28:217–26.
- Blankenberg FG. *In vivo* detection of apoptosis. *J Nucl Med* 2008;49 Suppl 2:81–95S.
- Patterson DM, Padhani AR, Collins DJ. Technology insight: water diffusion MRI—a potential new biomarker of response to cancer therapy. *Nat Clin Pract Oncol* 2008;5:220–33.
- Krishnan AS, Neves AA, de Backer MM, et al. Detection of cell death in tumors by using MR imaging and a gadolinium-based targeted contrast agent. *Radiology* 2008;246:854–62.
- Sharma R, Katz JK. Taxotere chemosensitivity evaluation in mice prostate tumor: validation and diagnostic accuracy of quantitative measurement of tumor characteristics by MRI, PET, histology of mouse tumors. *Technol Cancer Res Treat* 2008;7:175–86.
- Sierra A, Michaeli S, Niskanen JP, et al. Water spin dynamics during apoptotic cell death in glioma gene therapy probed by T1rho and T2rho. *Magn Reson Med* 2008;59:1311–9.
- Weihls D, Mason TG, Teitel MA. Bio-microrheology: a frontier in microrheology. *Biophys J* 2006;91:4296–305.
- Mason TG, Ganesan K, vanZanten JH, Wirtz D, Kuo SC. Particle tracking microrheology of complex fluids. *Phys Rev Lett* 1997;79:3282–5.
- Girard KD, Chaney C, Delannoy M, Kuo SC, Robinson DN. Dynacortin contributes to cortical viscoelasticity and helps define the shape changes of cytokinesis. *EMBO J* 2004;23:1536–46.
- Matzke R, Jacobson K, Radmacher M. Direct, high-resolution measurement of fur row stiffening during division of adherent cells. *Nat Cell Biol* 2001; 3:607–10.
- Beil M, Micoulet A, von Wichert G, et al. Sphingomylophosphorylcholine regulates keratin network architecture and visco-elastic proper ties of human cancer cells. *Nat Cell Biol* 2003;5:803–11.
- Shen HR, Spikes JD, Kopecková P, Kopecek J. Photodynamic crosslinking of proteins. II. Photocross-linking protein-ribonuclease A. *J Photochem Photobiol B* 1996;35:213–9.
- Spikes JD, Shen HR, Kopecková P, Kopecek J. Photodynamic crosslinking of proteins. III. Kinetics of the FMN- and rose bengal-sensitized photooxidation and intermolecular crosslinking of model tyrosine-containing N-(2-hydroxypropyl)methacrylamide copolymers. *Photochem Photobiol* 1999;70:130–7.
- Shen HR, Spikes JD, Kopecková P, Kopecek J. Photodynamic crosslinking of proteins. I. Model studies using histidine and lysine-containing N-(2-hydroxypropyl) methacrylamide copolymers. *J Photochem Photobiol B* 1996;34:203–10.
- Shen HR, Spikes JD, Kopecková P, Kopecek J. Photodynamic crosslinking of proteins. I. Model studies using histidine and lysine-containing N-(2-hydroxypropyl) methacrylamide copolymers. *J Photochem Photobiol B* 1996;34:203–10.
- Azrif M, Ranieri A, Giles A, Debeljevic B, Kolios M, Czarnota GJ. Conventional low-frequency ultrasound detection of apoptosis. *Proc Am Inst Ultra Med Annu Meeting* 2007;185.
- Feleppa EJ, Fair WR, Tsai H, et al. Progress in two-dimensional and three-dimensional ultrasonic tissue-type imaging of the prostate based on spectrum analysis and nonlinear classifiers. *Mol Urol* 1999;3:303–10.
- Huisman HJ, Thijssen JM. Precision and accuracy of acoustospectrographic parameters. *Ultrasound Med Biol* 1996;22:855–71.
- Lizzi FL, King DL, Rorke MC et al. Comparison of theoretical scattering results and ultrasonic data from clinical liver examinations. *Ultrasound Med Biol* 1998;14: 377–85.
- Oelze ML, Zachary JF. Examination of cancer in mouse models using high-frequency quantitative ultrasound. *Ultrasound Med Biol* 2006;32:1639–48.
- Oelze ML, Zachary JF, O'Brien WD, Jr. Parametric imaging of rat mammary tumors *in vivo* for the purposes of tissue characterization. *J Ultrasound Med* 2002;21:1201–10.